Shape deformations of surface-charged microdroplets

E. Giglio, B. Gervais, J. Rangama, B. Manil, and B. A. Huber
Centre Interdisciplinaire de Recherche Ions Lasers (CIRIL), CEA-CNRS-ENSICAEN Boîte Postale 5133, F-14070 Caen, France

D. Duft, R. Müller, and T. Leisner
Institut für Physik, Technische Universität Ilmenau, Postfach 100565, D-98684 Ilmenau, Germany

C. Guet
CEA/Saclay, F-91191 Gif-sur-Yvette, France

(Received 6 May 2007; revised manuscript received 18 December 2007; published 31 March 2008)

We present the deformation pathway of critically charged glycol and water droplets from the onset of the Rayleigh instability and compare it to numerical results, obtained for perfectly conducting inviscid droplets. In this simple model presented here, the time evolution of the droplet shape is given by the velocity potential equation. The Laplace equation for the velocity potential is solved by expanding the potential onto harmonic functions. For the part of the pathway dominated by electrostatic pressure, the calculations reproduce the experimental data nicely, obtained for both, glycol and water microdroplets. We find that the droplet shape and in particular the tips, just before charge emission, are well fitted by a lemon shape. We stress that the tip is tangent to a cone of 39° and thus significantly narrower than a Taylor cone.

DOI: 10.1103/PhysRevE.77.036319 PACS number(s): 47.20.Dr, 47.20.Ma

In 1882 Lord Rayleigh established the criteria for stability of a liquid, incompressible, charged droplet [1]. Rayleigh showed the spherical form characterized by an electrostatic energy E_C, and a surface energy E_S, is stable against all infinitesimal deformations insofar as the fissility parameter $X=E_C/2E_S$, is less than its critical value $Xc=1$. Here the droplet becomes unstable against an infinitesimal spheroidal deformation. When charging the droplet above this limit, Lord Rayleigh predicted the formation of fine jets without giving further details [1]. By charging to several thousand volts a drop of liquid standing at the lower end of a glass tube Zeleny observed for the first time the disintegration of charged drops [2]. His photographs show that when electrified to a critical limit the drop quickly deforms and the liquid is pulled out into a fine thread. Working with isolated charged bubbles, Sir G. Taylor was the first to point out that the drop elongates until it quickly develops an apparently conical end and that a narrow jet appears at the vertex [3]. Moreover Taylor realized that a conical point could exist in equilibrium and gave the condition for stationarity. Namely, the exact balance of capillary pressure and electrostatic pressure on a perfectly conducting conical fluid occurs only for an opening half-angle of 49.3°. Indeed formation of conical liquid meniscus and associated jet emission are complex fluid dynamical phenomena and still remain poorly understood in spite of detailed investigations [4–6]. It ought to be emphasized that the interest is not purely academic as the production of microsized or nanosized jets is of present considerable importance in modern technologies that require a fine control of the size of jets and their decay droplets. In passing we recall that Coulomb instabilities are fundamental in the nuclear fission process whose seminal explanation was actually inspired by the Rayleigh model, but which of course requires a genuine quantum mechanical treatment to account for most features [7,8]. Coulomb instabilities and fission of clusters of a few to thousands of atoms also been the object of numerous theoretical and experimental studies aiming in particular to understand the evolution from purely quantal behavior to the classical charged droplet features [9,10].

In recent experiments, we observed the time evolution of shape deformations of charged glycol microdroplets and the onset of charge-driven instabilities leading to the formation of fine jets [11–13]. Nowadays, highly resolved snapshots allow us to record in detail the deformation pathway of such a disintegration process, providing guide lines (constraints) to theoretical models. In this paper we present the deformation pathways of ethylene glycol and supercooled water droplets and compare them to numerical results obtained for an inviscid charged droplet. Relying on simulations, we show that the deformation pathway is quite general, while the details of the pathway depend on the viscosity and charge mobility of the liquid. Further, we discuss the droplet shape and the stress at its surface just before break up and identify the tip shape, from which fine jets are emitted.

I. EXPERIMENTAL SETUP

Individual droplets of water and ethylene glycol were generated on demand with a piezo driven nozzle, charged by influence from a high voltage electrode and injected into a thermostated electrodynamic balance operating at ambient pressure. The balance is of the classical "Paul-trap" design where a hyperboloidal torus electrode (radius $d=5$ mm) is capped by hyperboloidal top and bottom electrodes. As shown in Fig. 1, the torus electrode is machined from massive copper in the shape of an octagon, the faces of which carry the various optical and electrical ports. It is connected by copper braids to a cryostat which allows us to adjust the temperature of the levitator between −100 and +100 °C. The torus electrode is always kept at ground potential and carries the top and bottom electrode mounted on boron nitride insulators for optimal thermal contact. The droplets are levitated by applying an ac voltage with constant amplitude of 1500 V

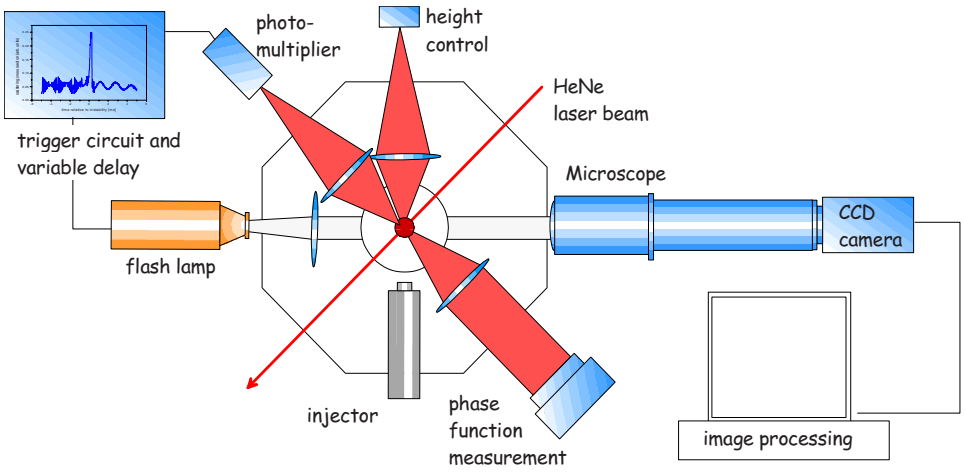

FIG. 1. (Color online) Schematic experimental setup (cross section through the levitator in the horizontal plane).

and variable frequency to the two endcap electrodes. In order to compensate the gravitational force on the droplet, an additional static field in vertical direction is applied by superimposing the ac voltage with dc voltages of opposite polarity at the top and bottom electrode. The whole levitator is mounted into a vacuum chamber for thermal insulation and placed inside a horizontally orientated long working distance microscope (Mitutoyo, 10× and 20× objectives used). This microscope is equipped with a triggerable flashlamp (HSP nanolight) for illumination and a cooled CCD camera (PCO Sensicam) for image acquisition (see Fig. 1).

A HeNe laser beam polarized at an angle of 45° with respect to the horizontal plane of scattering illuminates the droplet. Scattered light is used to image the droplet via a second microscope objective onto a vertically oriented linear CCD array in order to determine its vertical position in the trap. This position is stabilized by feeding back the vertical position information to the dc voltage applied to the endcap electrodes. From the magnitude of this voltage the mass-to-charge ratio of the droplet can be deduced. This value serves to adjust the frequency of the ac voltage to assure stable trapping as the droplets evaporate. Under typical conditions this frequency varies between 200 Hz and 1000 Hz. Light scattered from the droplet is detected angular resolved with a two-dimensional CCD camera for phase function measurements. Perpendicular polarizer segments in front of the camera allow recording simultaneously parallel and perpendicular polarized scattering. Thereby a time resolved determination of the droplet size is achieved with high accuracy [11] at a repetition rate of 12.5 Hz. A typical example of the size and charge of an evaporating glycol droplet is given in Fig. 2 as a function of time.

Additionally, a photomultiplier detector probes the overall intensity of the perpendicular polarized light scattered in an angular range between 80° and 100° at a much higher temporal resolution ($f_{\max}=25$ kHz). This signal is eventually used to detect the onset of a Coulomb instability, as described in more detail below. At the center of the levitator, the droplets are subjected to a time dependent electric potential of the form $\Phi(r,z,t)=V_0\frac{r^2-2z^2}{d^2}\cos(\omega t)$. This potential is responsible for the trapping of the droplets but also induces quadrupole shape oscillations of the extended surface charged droplet. These oscillations modulate the light scattering cross section of the droplets at the frequency of the trap and are therefore easily detected by the photomultiplier. Analyzing this modulation, we have been able to determine the amplitude and phase of the quadrupole oscillation and were thus able to confirm that the Coulomb instability coincides with a resonance between droplet and trap field and therefore does indeed occur at $X=1$ [12]. At the same time we observed that the instability itself is accompanied by a pronounced increase in light scattering intensity, as displayed in Fig. 3.

The figure shows, at negative times, the strongly modulated light scattering from the oscillating droplet before Cou-

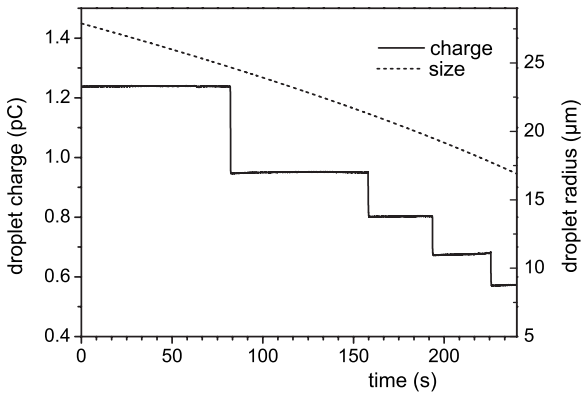

FIG. 2. Size and charge of an evaporating glycol droplet.

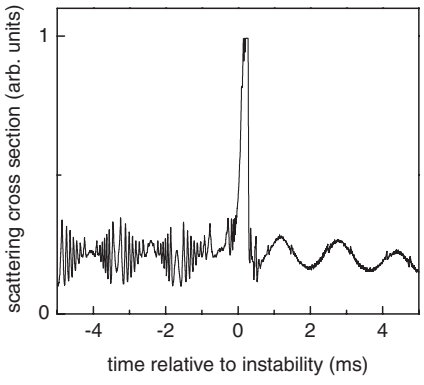

FIG. 3. Light scattering from an oscillating droplet in the vicinity of a Coulomb instability.

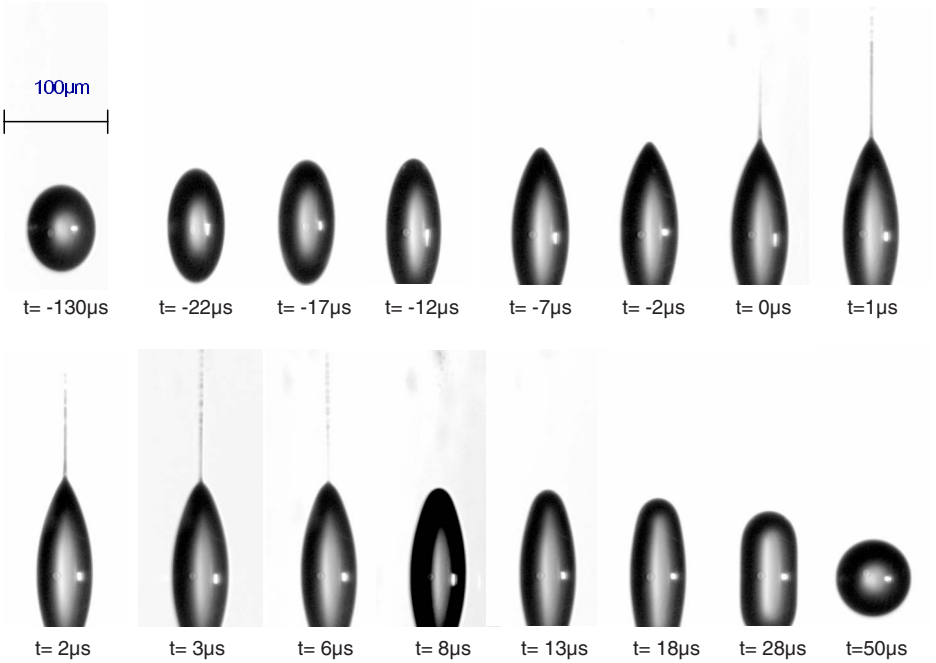

FIG. 4. (Color online) Snapshots showing the shape evolution of the glycol droplet of a radius of 32 μm after the onset of instability. Droplet's temperature is 85 °C. Jet emission is chosen as origin of time. The second jet at the bottom of the droplet form is not shown.

lomb instability. Around time zero we observe a Coulomb instability which is accompanied by a pronounced increase in light intensity. After the instability the droplet is less charged and oscillates at a much lower amplitude, which is reflected by the gentle modulation of the scattered light in phase with the ac drive voltage at positive times. The peak in light scattering is the result of a strong geometric deformation of the droplet and is used to determine the onset of a Coulomb instability. It allows us to activate the CCD camera attached to the long distance microscope and to trigger the flashlamp at a preset time delay after the detection of the instability. By repeating this procedure with subsequent droplets at increasing delay time we are able to analyze the process of the Coulomb instability with high temporal and spatial resolution.

In Fig. 4 we show an ethylene glycol droplet characterized by a radius of 24 μm carrying a charge of ~3.3 pC, at the onset of the Coulomb instability. This corresponds to the Rayleigh limit at $X=1$. After roughly 200 μs, the droplet is strongly deformed, its ellipsoidal shape has an aspect ratio larger than 2 (snapshot labeled $t=-22$ μs of Fig. 4). This value increases further within the next 20 μs to about 3.5, when two tips are formed and two jets are ejected at opposite sides of the droplet. Within a time duration of about 4 μs the system loses about 1/3 of the charge, without any essential mass loss ($<0.5\%$). The discontinuities, which appear within the jets, indicate the formation of small segments and later on small charged droplets with a diameter of about 1 to 2 μm. Within experimental resolution, we cannot determine here with certainty if the jets are emitted from well defined conical ends or not. In any case, the observed tip seems close to a cone with a half-angle estimated here to ~30°.

After charge emission, the deformed droplet relaxes to its spherical form nearly twice as fast as the original deformation has required. However, it does not follow the ellipsoidal shapes but rather those of an elongated capsule (see $t=+28$ μs). In Fig. 5 we show the disintegration of a water droplet characterized by a radius of 35 μm. The process is almost 2 times faster than for the glycol droplet but it appears that the droplet deformation pathway, from instability to break up and back to the initial spherical form, is quite general, even if the details of the pathway (mainly the last part) should be attributed to dynamical properties of the fluid.

II. THE MODEL

For a better understanding of the observed phenomena, we simulate the evolution of a critically charged droplet from the Coulomb instability up to fission and back to the initial sphere. The model is not intended for describing the fission itself (the jets of charged matter at both tips) but merely the nonlinear evolution that develops after the onset of the Coulomb instability. The liquid is assumed to be inviscid and incompressible with an irrotational flow. The latter implies that the velocity field $\mathbf{v}$ of the fluid can be defined as the gradient of a scalar function ψ, $\mathbf{v}=\nabla\psi$. Together, these assumptions yield $\Delta\psi=0$, which ensures that the evolution of the droplet occurs at constant volume, while ignoring viscous properties of the fluid. The liquid is considered to be perfectly conducting so that the Coulomb potential V is constant all over the surface. The surface charge density σ is then proportional to the normal derivative of the electric potential V outside the surface. Finally, we assume axisymmetry for the shape and assign θ to the polar angle, the origin coinciding with the droplet center. Within these hypotses, the droplet deformation is described by the time evolution of the surface vector $\mathbf{s}(\theta,t)$. Note that, unlike Betelù *et al.* [14] who studied the shape deformation using the Stokes equation, we discard the 0viscosity term but include the inertial term of the Navier-Stokes equation, allowing for dynamical effects. We introduce the characteristic deformation time scale $\tau=\sqrt{\rho R_0^3/\gamma}$, with R_0, ρ, γ being the initial droplet radius, density, and surface tension, respectively. This allows defining

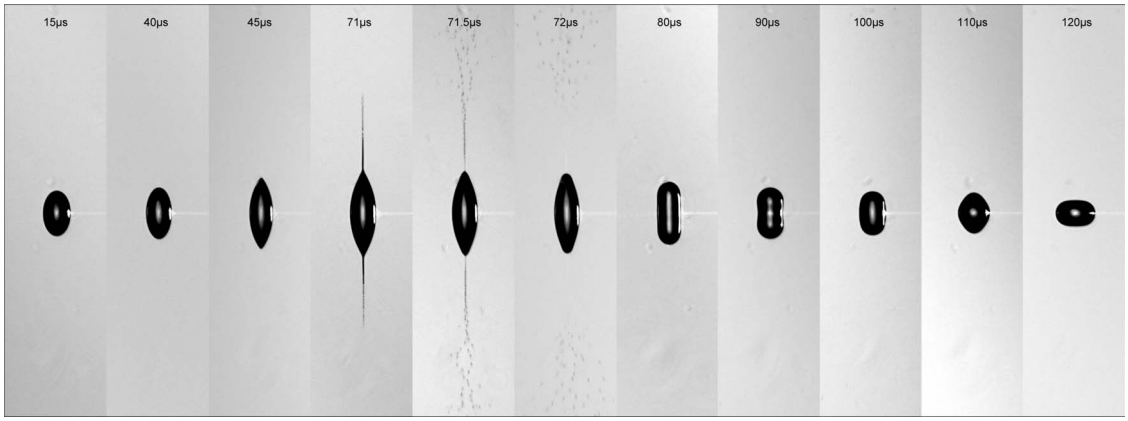

FIG. 5. Snapshots showing the shape evolution of a supercooled water droplet (−5 °C) with a radius of 35 μm after the onset of instability.

the following dimensionless quantities: $t \to t\tau$, $\psi \to \psi \frac{R_0^2}{\tau}$, $\sigma \to \sigma \sqrt{\frac{4X\gamma\epsilon_0}{R_0}}$, $H \to H/R_0, \ldots$, and to describe the surface dynamics by a set of dimensionless equations [15]

$$\Delta V = 0 \ \mathbb{R}^3 \setminus \Omega, \quad \sigma = \frac{\partial V}{\partial n} \text{ on } \partial\Omega,$$

$$\Delta\psi = 0 \text{ in } \Omega,$$

$$\frac{\partial\psi}{\partial t} + \frac{\mathbf{v}^2}{2} + 2H - 2X\sigma^2 = 0 \text{ on } \partial\Omega,$$

$$\frac{d\mathbf{s}}{dt} = \mathbf{v} = \boldsymbol{\nabla}\psi \text{ on } \partial\Omega. \tag{1}$$

The quantity H stands for the mean curvature of the droplet surface. In order to calculate the fluid velocity at the surface, we have to solve the Laplace equation for ψ inside the droplet volume Ω with the boundary condition given by Eq. (1). As $\Delta\psi=0$, ψ can be written as a linear combination of harmonic functions, having the correct behavior close to the origin. We choose to solve the Laplace equation in the prolate spheroidal coordinate system (η, ζ, ϕ), as it is well adapted to our boundary problem, while the harmonic functions $f_{n,m}$ are still separable

$$f_{n,m}(\eta, \zeta, \phi) = \sum_{n,m} a_{n,m} P_n(\eta) P_n^m(\zeta) e^{im\phi},$$

where P_n^m is a Legendre polynomial of order n and degree m [16]. Assuming axial symmetry, $m=0$ and the expansion coefficients $\{a_n\}$ are chosen such as to satisfy the boundary conditions

$$\psi(\zeta_i) = \sum_n a_n P_n[\eta(\zeta_i)] P_n(\zeta_i). \tag{2}$$

Here, the vector $\{\eta(\zeta_i), \zeta_i\}$ describes the droplet surface in the prolate coordinate system. As the boundary conditions change in time, the set of linear equations must be solved at each time step. A similar technique is used to calculate the Coulomb potential V outside the droplet. We used 600 angular points ζ_i and a maximum of 200 harmonic functions. Careful testing of the results convinced us that we were using a sufficient number of terms. As we consider here a perfectly conducting, inviscid liquid, the fissility parameter X is the only free parameter of the model that influences the pathway. The quantities R_0, ρ, and γ define merely the time scale τ of the droplet deformation. The latter is therefore quite general within the given hypotheses.

III. COMPARISON BETWEEN EXPERIMENTAL AND SIMULATED RESULTS

In Fig. 6, we show snapshots of the simulation before ($X=1$) and after charge emission ($X=0.5$). The starting point is a critically charged prolate spheroid of an eccentricity of $e=0.2$ (almost spherical drop). We see that the model is able to reproduce with high quality the whole sequence of the nonlinear deformation dynamics of a critically charged droplet. In particular, for X=1, we end up with the same spindlelike form as the glycol droplet (see Figs. 4 and 6). At the moment, when the droplet starts to form a jet at the tips (snapshot labeled by time $t=0$), we reduce the charge by $\sim$30% by changing suddenly the fissility to $X=0.5$. This allows us to simulate the charge emission and to describe the shape deformation after it, without stopping the calculation. After emission, the droplet retracts similarly to experimental data, adopting a capsulelike form, which, however, initially has a bulge in the middle. The model also shows some weaknesses. The lack of viscosity hinders the dissipation of the excess of potential energy obtained during charge emission. The model is therefore not able to describe the deformation back to equilibrium shape (sphere). Further, as viscosity slows down the flow, we expect that the deformation time we get from simulation underestimates the experimentally observed one. Indeed, glycol droplets such as the one shown in Fig. 4, with $\{\rho, \gamma(85\ ^\circ\text{C}), R_0\} = \{1.1\ \text{g/cm}^3, 43\ \text{mN/m}, 32\ \mu\text{m}\}$, have a characteristic time scale of $\tau = 29\ \mu$s. From Fig. 4 we note that the glycol droplet needs 130 μs to attain the spindlelike shape (starting from an already prolate spheroid of $e=0.745$), while the simulation gives $2.25\tau = 65.1\ \mu$s. Compared to the observed 130 μs, it

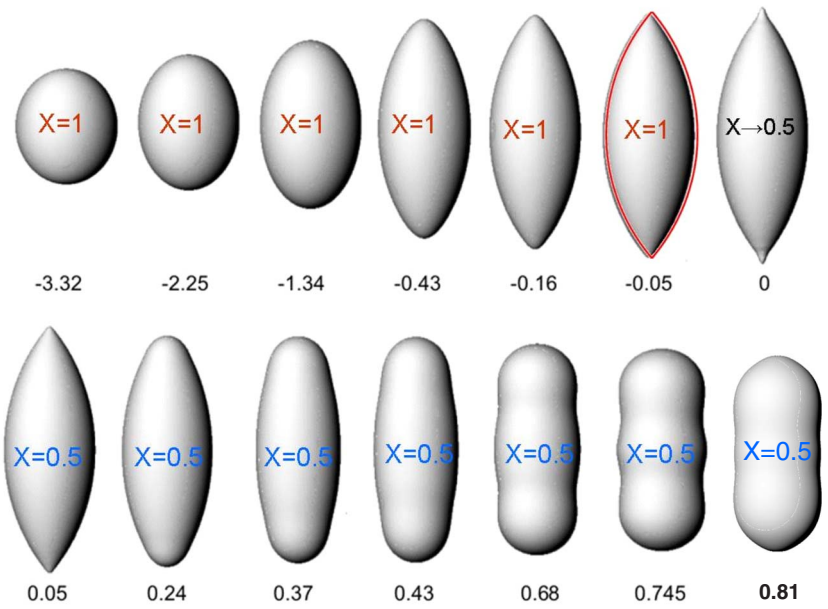

FIG. 6. (Color online) Calculated shape sequence of an initially critically charged droplet ($X=1$), experiencing charge emission ($X=0.5$) at the moment a bulb appears at the tip. Physical times are obtained by multiplying dimensionless times t, shown under each shape, by the characteristic time τ of a given droplet. Fluid is nonviscous and perfectly conducting. Charge emission is chosen as origin of time. The red lemon-fit has been slightly shifted for better comparison.

is almost 2 times faster. For the supercooled water droplets shown in Fig. 5, jet emission occurs after only 70 μs. Having a characteristic time of $\tau=23$ μs, we obtain a simulated deformation time of $2.25\tau=53$ μs. The difference is thus much smaller, which we assign to their lower viscosity.

Nevertheless, the model allows access to the shape and in particular to the tip of the droplet just before surface breakup. Up to now, it was unknown whether the jets are emitted from a Taylor cone [3] as assumed by de la Mora [17], likely to electrosprays [3,18], or rather from a hyperboloidal tip as was pointed out by Yarin *et al.* [19] in the case of sessile and pendant droplets in an electric field. When zooming on the tip, we note that the jets are not emitted from a conical tip, but at best from a hyperboloid which is tangent to a cone of 33°. Yarin *et al.* showed that the maximal electric potential at which a stationary infinite hyperboloid can exist, corresponds to a hyperboloid tangent to a cone of 33.5° [19]. This critical hyperboloid was the starting point from which jets are formed from pendant droplets for increasing electric fields. Interestingly, it is close to the hyperboloid that best fits the tip, hinting that the last one is close to break-up. Nevertheless, in our case, the hyperboloid is not a satisfying fit either, in the sense that it only fits the tip, instead of the whole droplet. We looked for a geometrical description of the whole shape, just before charge emission, and found that the droplet is remarkably well fitted by a "lemon" of equation $z^2=A^2-(B+r)^2$, $A=3.02$, $B=2.25$, with $r=\sqrt{x^2+y^2}$ being the distance from the symmetry axis. Note that the fit has only one free parameter as A and B are related by the volume constraint. The lemon is shown in the upper inset of Fig. 7 as a red contour. When zooming on the tip, we see only a small discrepancy close to the apex (lower inset of Fig. 7). We deduce that the tip is tangent to a cone of 39°, thus significantly narrower than the Taylor cone (49.3°) but larger than the one obtained by Betelù *et al.* (cone of 25°) for a viscous droplet [14]. The experimentally observed tip's opening half-angle of 30° lies between both predictions. The lemon may be considered as the asymptotic shape of a critically charged droplet, if breaking up could be hindered.

For further analysis of the tip behavior, we introduce the local fissility $x(\theta)$ defined as the Coulomb pressure divided by the pressure due to the surface tension, $x(\theta)=X\sigma^2(\theta)/H(\theta)$. In order to be able to break up the surface, the Coulomb pressure must outbalance the stress due to the surface tension $x(\theta)>x_c\geq 1$, where the critical local fissility x_c still needs to be determined. For a spheroid, the Coulomb pressure can be expressed as a function of the Gaussian curvature K of the surface [20], yielding $x(\theta)=X\sqrt{K(\theta)}/H(\theta)$. As for spheroids, $H^2\geq K$, independently of the eccentricity

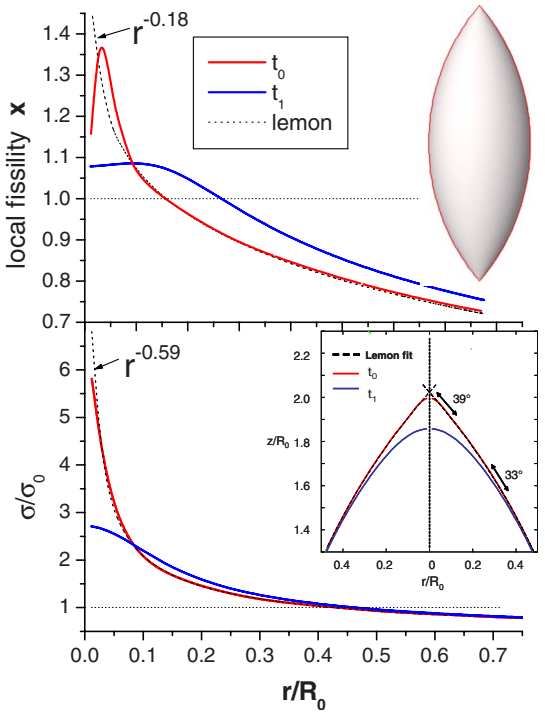

FIG. 7. (Color online) Local fissility x and charge density of the droplet at two different times $t_0=-0.05$ and $t_1=-0.43$ just before jet emission. Dashed line stands for the lemon shape. Insets show the fit of the droplet by a lemon shape (red contour).

[20], the local fissility of critically charged spheroids ($X=1$) cannot exceed the unit [$x(\theta) \leq 1$] and jets cannot appear at their ends, even for large eccentricities. Critically charged lemons, however, behave differently as the local fissility is no longer bound and can exceed one at the tips. Indeed, for the lemon tip shape depicted in Fig. 7, the surface charge density diverges close to the apex as $\sigma(r \to 0) \propto r^{-0.59}$, while the mean curvature diverges as $H(r \to 0) \propto r^{-1}$(not shown). Hence, the local fissility diverges at the apex as $x(r \to 0) \propto r^{-0.18}$. Such critically charged lemon shapes lead therefore inevitably towards surface break up of the tip.

In Fig. 7, we give the local fissility (upper panel) and charge distribution (lower panel) of the droplet at different times (shapes) before charge emission and compare them to the one calculated for the lemon shape. As soon as the shape deviates from a spheroid to become rugbyball-like (around $t_1=-0.43$), the local fissility exceeds 1 at the tips [$x(0)=1.08$]. This shows that the local fissility can reach values larger than 1 at nonsingular surface points. However, this also shows that $x > x_c=1$ is not a sufficient criterion for surface break-up but indicates rather the less stable region. At time $t_0=-0.05$, the charge distribution compares well to the charge distribution on the lemon surface except that it stays bounded at the apex. At that moment, the electric field at the tip is about 6 times larger than initially. Finally, a bulb appears at the tip, which indicates the formation of a jet.

The simulated sequence is quite general for inviscid perfectly conducting liquid droplets. However, dynamical properties of the fluidlike viscosity and charge mobility may change the details of the deformation dynamics. Indeed, unlike metallic droplets, for which the charge mobility is infinite, the charge mobility in polar liquids is due to ionic mobility and thus related to the viscosity of the fluid and the shape and size of the ion. Thus, for polar liquids like water and glycol the Coulomb pressure on the droplet surface may significantly deviated such as the one of a perfectly conducting droplet. In order to compare easily the pathways of different droplets, the shapes have been fitted with a superspheroid of the form $(z^2/a^2)^{n/2}+[(x^2+y^2)/b^2]^{n/2}=1$ with the constraint of constant volume. Superspheroids can either fit capsule or spindlelike forms, depending on n, so that the whole droplet deformation can be represented reasonably well on a 2D graph. The exponent n is shown as a function of the aspect ratio (a/b) at different deformation times. First consider the experimental glycol and water results, shown in Fig. 8. We find that the general behavior is similar in both cases: the instability starts with increasing a/b, while n remains nearly constant at $n \approx 2$, meaning that the initial deformation remains mainly prolate spheroidal. Then n decreases and the form becomes spindlelike. The charge emission occurs at $a/b \sim 3.2$ to 3.5 with an n value of 1.4 to 1.6. After emission, the system retracts, while n increases quickly well above 2 to fit an elongated capsule, before both parameters come back to their initial values. The return can be monotone or oscillatory, depending on the fluid properties. Indeed, the water droplet exhibits a double oscillatory behavior between an oblate and prolate ellipsoid and between sharp and flattened ends. For glycol, the amplitudes of this motion are much smaller than for water, as dissipation is much stronger.

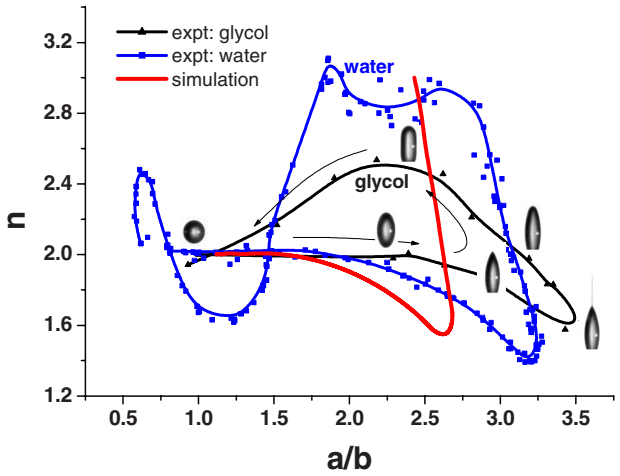

FIG. 8. (Color online) Comparison between simulated pathways (red) with experimentally observed deformation paths for glycol (black triangles) and undercooled water (blue squares) droplets. The aspect ratio a/b and exponent n correspond to a shape fitted with a superspheroid.

We add the simulated pathway to Fig. 8 and compare it to the experimental data. The simulation should well describe the deformation of a critically charged mercury droplet, which has low viscosity and is an excellent conductor. It predicts that the pointed ends are formed for a ratio $a/b=2.6$, which is significantly lower than the values obtained for water ($a/b=3.2$) and glycol ($a/b=3.5$). As the comparison does not hold even for low-viscous water droplets, we expect that the difference is due to the finite charge mobility of polar liquids. Work on the influence of the charge mobility on the pathway is underway. After charge emission, the deformation is mainly driven by the surface tension. The latter tends first to flatten the tips (capsule) before it drives the shape towards a sphere. In fact, the slope of the simulated curve after charge emission compares well to the experimental low-viscous water curve. As mentioned before, the model cannot describe the way back to the equilibrium shape and we stop the simulation when $n=3.2$. However, the comparison with the experimental curve for glycol fails, highlighting the role of viscosity and charge mobility. We deduce that after charge emission, the details of the pathway are dominated by viscous properties of the fluid and, thus, poorly described by the present model. Nevertheless, the simulation gives the limiting slope of the curve that cannot be overcome by real fluids.

IV. CONCLUSION

In conclusion, we have studied the deformation dynamics of critically charged microdroplets from an experimental and theoretical point of view. We showed that the whole shape sequence is well reproduced in the case of an inviscid fluid. Our work indicated that critically charged low-viscous metallic droplets (not yet observed) exhibit less elongated shapes than polar liquids such as water and glycol. It also showed that the jets are not emitted from a Taylor cone, as for electrosprays, but rather from lemonlike tips. This is con-

firmed by the analysis of the local fissility, which diverges at the tip apex. Finally we found that the deformation path follows always the same pattern independently of the static properties of the droplet: density, surface tension, size. Nevertheless, comparisons with experimental data highlight the importance of the viscosity and charge mobility of the liquid on the details of the pathway. In particular, differences in the pathways of low-viscous fluids such as water are therefore expected to be due to finite charge mobility. Work in this direction is underway.

[1] Lord Rayleigh, Philos. Mag. **14**, 184 (1882).
[2] J. Zeleny, Phys. Rev. **10**, 1 (1917).
[3] Sir G. Taylor, Proc. R. Soc. London, Ser. A **280**, 383 (1964).
[4] J. F. de la Mora, Annu. Rev. Fluid Mech. **39**, 217 (2007).
[5] M. Cloupeau and B. Prunet-Foch, J. Electrost. **22**, 135 (1989).
[6] C. Pantano, A. M. Gañán-Calvo, and A. Barrero, J. Aerosol Sci. **25**, 1065 (1994).
[7] N. Bohr and J. A. Wheeler, Phys. Rev. **56**, 426 (1939).
[8] W. J. Swiatecki, Phys. Rev. **104**, 993 (1956).
[9] U. Näher, S. Bjørnholm, S. Frauendorf, F. Garcias, and C. Guet, Phys. Rep. **285**, 245 (1997).
[10] P. Blaise, S. A. Blundell, C. Guet, and Rajendra R. Zope, Phys. Rev. Lett. **87**, 063401 (2001).
[11] D. Duft, H. Lebius, B. A. Huber, C. Guet, and T. Leisner, Phys. Rev. Lett. **89**, 084503 (2002).
[12] D. Duft, T. Achtzehn, R. Müller, B. A. Huber, and T. Leisner, Nature (London) **421**, 128 (2003).
[13] T. Achtzehn, R. Müller, D. Duft, and T. Leisner, Eur. Phys. J. D **34**, 311 (2005).
[14] S. I. Betelu, M. A. Fontelos, U. Kindelan, and O. Vantzos, Phys. Fluids **18**, 051706 (2006).
[15] O. A. Basaran and L. E. Scriven, Phys. Fluids A **1**, 5 (1989).
[16] P. M. Morse and H. Feshbach, *Methods of Theoretical Physics* (McGraw-Hill, New York, 1953), Pt. I, p. 661.
[17] J. F. de la Mora, J. Colloid Interface Sci. **178**, 209 (1996).
[18] J. B. Fenn, M. Mann, C. K. Meng, S. F. Wong, and C. M. Whitehouse, Science **246**, 64 (1989).
[19] A. L. Yarin, S. Koombhongse, and D. H. Reneker, J. Appl. Phys. **90**, 4836 (2001).
[20] I. W. McAllister, J. Phys. D **23**, 359 (1990).